Supporting Information

CRISPR-Cas9 mediated DNA unwinding detected using site-directed spin labeling

Narin S. Tangprasertchai,[1] Rosa Di Felice,[2,3,4] Xiaojun Zhang,[1] Ian M. Slaymaker,[5] Carolina Vazquez Reyes,[1] Wei Jiang,[1] Remo Rohs,[1,2,3] and Peter Z. Qin[1,3,*]

[1]Department of Chemistry, [2]Department of Physics and Astronomy, and [3]Department of Biological Sciences, University of Southern California, Los Angeles, CA 90089, USA

[4]Center S3, CNR Institute of Nanoscience, Via Campi 213/A, 41125 Modena, Italy

[5]Broad Institute of MIT and Harvard, Cambridge, MA 02142, USA

Table of Contents

S1. Materials and Methods

S1.1: Streptococcus pyogenes *Cas9 protein expression and purification*

Cas9 from *Streptococcus pyogenes* (referred to as Cas9 throughout) was expressed and purified following reported procedures.[1, 2] pET-based T7 promoter-containing plasmids encoding the wild-type Cas9 and the catalytically inactive variant (dCas9) were obtained from Addgene (http://www.addgene.org) (pMJ806 for Cas9 and pM841 for dCas9). The plasmids encode a fusion protein construct containing an N-terminal His_6 tag followed by maltose-binding protein (MBP) tag, a tobacco etch virus (TEV) protease cleavage site, and the Cas9 sequence spanning residues 1–1368. The dCas9 contains mutations of D10A and H840A, which reside at the active sites of the RuvC and HNH nuclease domains, respectively. The plasmids were transformed into competent *E. coli* strain BL21-Gold(DE3)pLysS (Agilent Technologies) using a heat shock treatment, then grown overnight at 37 °C on Luria broth (LB) agar containing 25 μg mL^{-1} kanamycin (kan). The presence of the correct plasmid was confirmed by DNA sequencing.

To overexpress the protein, a single colony from the transformation was inoculated in 50 mL LB with 25 μg/mL kan and incubated at 37 °C with ~225 rpm shaking overnight, which was subsequently used to inoculate a large-scale culture (typically 8 mL of culture in 500 mL LB with 25 μg/mL kan). The large-scale culture was incubated at 30 °C with ~225 rpm shaking, and cell growth was monitored by measuring optical density at 600 nm (OD_{600}). Once OD_{600} reached ~0.8, the temperature was reduced to 18 °C, and protein overexpression was induced by the addition of isopropyl β-D-1-thiogalactopyranoside (IPTG) to a final concentration of 200 μM. The culture was then incubated at 18 °C with ~225 rpm shaking overnight. Upon conclusion of overexpression, the cells were harvested using centrifugation, then either lysed immediately or flash frozen in liquid nitrogen and stored at –80 °C.

The cell pellet was resuspended in ice-chilled lysis buffer (20 mM Tris–HCl, pH 8.0, 250 mM NaCl, 5 mM imidazole, 5 mM β-mercaptoethanol (BME); ~ 15 ml per 1 L culture), then lysed by sonication in the presence of protease inhibitor, on ice. Following cell lysis, the protein was purified using Ni-NTA affinity and cation-exchange chromatography at 4 °C. The clarified supernatant, which contains the desired soluble protein, was incubated with Ni-NTA resin (QIAGEN), then loaded onto a filter screening column (UriSys 5mL, Fisherbrand®). Once the protein/Ni-NTA resin was packed, the column was washed with the lysis buffer, followed by lysis buffer with 10mM and then 20mM imidazole. The protein was eluted using lysis buffer containing 200mM imidazole. The protein containing fractions were pooled, and salt concentrations were adjusted using 20mM Tris-KOH (pH 7.5), 5% (v/v) glycerol, and 5 mM BME (buffer A). The protein was further purified via fast protein liquid chromatography (FPLC) using a MonoS HR5/5 cation-exchange column (GE Healthcare), with the low-salt buffer being buffer A and the high-salt buffer being 20 mM Tris-KOH (pH 7.5), 1 M KCl, 5% (v/v) glycerol, and 5 mM BME (buffer B). Elutions from the MonoS column were analyzed via sodium dodecyl sulfate polyacrylamide gel electrophoresis (SDS-PAGE), and the fractions containing the Cas9 proteins were pooled, then dialyzed against storage buffer (20 mM Tris-KOH, pH 7.5, 200 mM KCl, and 5% glycerol) to remove BME. After dialysis, the protein was concentrated using a 30 kDa molecular weight cutoff (MWCO) centrifugal filter (Amicon). Tris(2-carboxyethyl)phosphine (TCEP) was added to the concentrate to a final concentration of 0.5 mM before the protein was aliquoted, flash frozen in liquid nitrogen, and stored at –80 °C. Concentration of the protein stock was determined using UV-Vis absorbance at 280nm and extinction coefficient ε = 120,500 M^{-1} cm^{-1}, or by a Bradford assay.

Note that in the studies reported here, the His_6 and MBP tags were not cleaved. Previous studies have shown these tags do not interfere with Cas9 function.[3]

S1.2: RNA preparation

The single-guide RNA (sgRNA, see Table S1 for sequence) was synthesized by T7 *in vitro* transcription following previous reported procedures.[1, 4] The double-stranded DNA template for transcription was prepared by polymerase chain reaction (PCR). A typical 1 mL PCR reaction contained 1–3 µg of purified single-stranded sgDNA, 0.7 µM primer 1 and 0.7 µM primer 2 (see Table S1 for sequences), 200 µM each dNTP, 50 units Taq DNA polymerase (New England Biolabs, Inc.), and 1X Taq Buffer (New England Biolabs, Inc.). Upon conclusion of the reaction, the presence of the correct DNA product was confirmed by agarose gel, and the product was purified using the GeneJET PCR Purification Kit (ThermoScientific, Inc.).

A typical sgRNA transcription reaction (2 mL) contained 0.05 µM double-stranded DNA template, 750 µM each NTP, 40 mM Tris pH 7.5, 15 mM $MgCl_2$, 2 mM spermidine, 5 mM dithiothreitol (DTT), 0.01% triton, and T7 RNA polymerase. The reaction mixture was incubated at 37 °C for 3 hours, then stopped with the addition of EDTA to a final concentration of 20 mM. The transcription products were recovered by ethanol precipitation, then purified using denaturing polyacrylamide gel electrophoresis (PAGE). The purified sgRNA was resuspended in ME buffer (10 mM 3-(N-morpholino)propanesulfonic acid (MOPS) pH 6.5 and 1 mM EDTA) and stored at –20 or –80 °C. The concentration of sgRNA was determined by its absorbance at 260 nm using the extinction coefficient listed in Table S1.

Table S1: Oligonucleotides used in the preparation of sgRNA.

Name	**Sequence (5' → 3')**	**ε ($M^{-1}cm^{-1}$)**
sgRNA	GUGAUAAGUGGAAUGCCAUGGUUUUAGAGCUAGAAAUAGCAAGUUAAAA UAAGGCUAGUCCGUUAUCAACUUGAAAAAGUGGCACCGAGUCGGUGCUU	980,000[(a)]
sgDNA[(b,c)]	AAAAGCACCGACTCGGTGCCACTTTTTCAAGTTGATAACGGACTAGCCT TATTTTAACTTGCTATTTCTAGCTCTAAAACCATGGCATTCCACTTATC ACTATAGTGAGTCGTATTA	1,119,300
primer 1[(c)]	AAAAGCACCGACTCGGTG	178,800
primer 2[(c)]	TAATACGACTCACTATAG	189,000

(a) Estimated using an extinction coefficient of 10,000 M^{-1} cm^{-1} per nucleotide.
(b) T7 promoter underlined
(c) Obtained commercially from Integrated DNA Technologies, Inc.

S1.3: DNA spin labeling

The CRIPSR-Cas9 target DNA duplex used in this study was designated as p5, with the two individual strands being p5c (complementary to the guide segment of the sgRNA) and p5n (non-complementary to the guide segment of the sgRNA) (Table S2). These oligonucleotides were synthesized by solid-phase chemical synthesis (Integrated DNA Technologies,). If required, a phosphorothioate modification was incorporated at the designated site during chemical

synthesis, allowing for subsequent attachment of a spin label using the nucleotide-independent scheme procedure reported previously.[5-7]

Typically, a spin labeling reaction (100 µL) contained 0.1–1 mM crude phosphorothioate-modified oligonucleotide, 150 mM 3-iodomethyl-1-oxyl-2,2,5,5-tetramethylpyrroline (gift from Kálmán Hideg, University of Pécs, Hungary), 40% (v/v) acetonitrile, and 100 mM 2-(*N*-morpholino)ethanesulfonic acid (MES) pH 5.8. The reaction mixture was incubated at room temperature in the dark with constant mixing for 16–24 hours. The spin-labeled DNA was purified by anion exchange high-performance liquid chromatography (HPLC) with a DNAPac PA-100 column and desalted by reverse phase HPLC with a Prosphere C18 column.[5] The labeled DNA fractions were lyophilized and resuspended in ME buffer, and concentrations were determined by absorbance at 260 nm using extinction coefficients listed in Table S2.

Note that in this work the R_p and S_p phosphorothioate diastereomers present at each attachment site were not separated. Previous studies have validated the use of R_p/S_p mixtures in DEER measurement and established an appropriate method for interpreting the measured inter-nitroxide distances.[6, 8]

Table S2: CRISPR-Cas9 target DNAs used in this study

Name	Sequence (5' → 3')	ε ($M^{-1}cm^{-1}$)
p5c[(a)]	GCTCAATTTTGACAGC***CCA***CATGGCATTCCACTTATCACTGGCATCCTTCCACTC	495,800
p5c19[(a,b)]	GCTCAATTTTGACAGC***CC*A***CATGGCATTCCACTTATCACTGGCATCCTTCCACTC	
p5c33[(a,b)]	GCTCAATTTTGACAGC***CCA***CATGGCATTCCAC****T***TATCACTGGCATCCTTCCACTC	
p5n[(c)]	GAGTGGAAGGATGCCAGTGATAAGTGGAATGCCATG***TGG***GCTGTCAAAATTGAGC	554,700
p5n26[(b,c)]	GAGTGGAAGGATGCCAGTGATAAGT****G***GAATGCCATG***TGG***GCTGTCAAAATTGAGC	
tp5n26[(b,d)]	GTGATAAGT****G***GAATGCCATG***TGG***GCTGTCAAAATTGAGC	389,000

(a) Target strand. The protospacer segment is underlined, and the PAM nucleotides are indicated with bold italicized letters.
(b) "*" indicates the phosphorothioate modification site, at which the R5a spin label was later attached.
(c) Non-target strand. The protospacer segment is underlined, and the PAM nucleotides are indicated with bold italicized letters.
(d) A truncated non-target strand. The protospacer (underlined) and the PAM (bold italicized) are preserved, while the 5' segment forming the PAM-distal base-paired arm has been deleted.

S1.4: Complex assembly and characterization

A target DNA duplex was annealed by combining appropriate amounts of p5c and p5n strands, heating at 95 °C for 1 minute, cooling to room temperature for 1 minute, then incubating in an annealing buffer (50 mM Tris pH 7.5 and 100 mM NaCl) at either room temperature for a minimum of 1 hour or 4 °C overnight.

To assemble a Cas9/sgRNA complex, an appropriate amount of sgRNA in (ME buffer or water) was first heated at 95 °C for 1 minute and then cooled at room temperature for 1 minute. An appropriate amount of salt was added to the sgRNA so that the solution contained 20 mM Tris pH 7.5, 150 mM KCl, 5 mM $MgCl_2$, 5% (v/v) glycerol, and 0.5 mM TCEP (buffer R), and the mixture was incubated at room temperature for 15 minutes. This pre-folded sgRNA was then combined with an appropriate amount of protein (Cas9 or dCas9) folded in buffer R, and the mixture was incubated at room temperature for 30 minutes.

For binding of the target DNA to the Cas9/sgRNA complex, an appropriate amount of pre-formed p5 duplex was incubated with the pre-assembled Cas9/sgRNA complex in buffer R. The mixture was then incubated at 37 °C for 30 minutes.

Complex assembly was characterized using native PAGE at 4 °C under 89 mM Tris-HCl pH 7.5, 89 mM boric acid, and 5 mM $MgCl_2$. Nucleic acid species were visualized by ethidium bromide (EtBr) staining.

S1.5: CRISPR cleavage assay

To monitor DNA cleavage by Cas9, an individual p5c or p5n strand was first radiolabeled following a previously reported protocol.[9] A typical 10-µl radiolabeling reaction contained 1 µM DNA (either unlabeled or R5a-labeled), 1 µL ^{32}P γ-ATP (MP Biomedicals, Inc.), 10 units T4 polynucleotide kinase (PNK, New England Biolabs, Inc.), and 1X PNK Buffer (New England Biolabs, Inc.). The mixture was incubated at 37 °C for 30 minutes, then the T4 PNK was heat deactivated by incubation at 65 °C for 20 minutes. As previous studies have indicated that denaturing PAGE may cause some loss of the spin label,[5] the ^{32}P-labeled strands were not gel purified. Instead, following PNK inactivation, an equimolar amount of the complementary DNA strand was added to the sample. The mixture was incubated at room temperature for 1 hour to allow p5 duplex formation and then passed through a 10 kDa MWCO centrifugal filter (Amicon Ultra) to remove the majority of free ^{32}P γ-ATP.

Cleavage of p5 DNA by Cas9/sgRNA was monitored under single turnover conditions. Reactions were carried out in buffer R, and were initiated by adding an appropriate amount of p5 (~100 nM, doped with ^{32}P-labeled duplexes prepared as described above) to Cas9/sgRNA complexes (350 nM) pre-assembled as described above. The reaction mixtures were incubated at 37 °C for 30 minutes, then stopped with the addition of urea and EDTA to final concentrations of 6 M and 2 mM, respectively. The products were resolved with 10% denaturing PAGE. Gels were dried and quantified by autoradiography using a Bio-Rad Personal Molecular Imager and QuantityOne software (Bio-Rad #1709600).

S1.6: EPR sample preparation

EPR samples were prepared following the same general procedure described below, with the amount of spin-labeled DNAs adjusted as described in sections on continuous-wave (cw) EPR and double electron-electron resonance (DEER) spectroscopy. The p5 duplexes were annealed in buffer R as described above from equimolar amounts of the appropriate complementary strands, with the typical DNA duplex concentration ranging from ~0.5–2 µM.

The complex-bound DNA samples were assembled with a 1:2:3 ratio of p5 duplex to sgRNA to Cas9, following the procedures described in S1.4: Complex assembly and characterization. Complex assembly was initiated in a large volume (~500–3000 µL), so that the concentrations of the DNA, sgRNA, and Cas9 protein were kept in the low µM range, as those used in the

binding and cleavage assays. Upon conclusion of complex assembly, the solution was concentrated to ~15–20 µL using a 100kDa MWCO centrifugal filter (Amicon Ultra) at 4 °C.

S1.7: Continuous-wave (cw) EPR spectroscopy

S1.7.1: Spectral Acquisition

Each sample was approximately 5 µL with the spin-labeled DNA concentration of approximately 40 µM. The sample was loaded into a borosilicate glass capillary (0.64mm ID x 0.84mm OD, Fiber Optic Center, Inc.) sealed at one end. X-band EPR spectra were acquired at room temperature on a Bruker EMX spectrometer using an ER4119HS cavity. The incident microwave power was 2 mW, and the field modulation was 3 G at a frequency of 100 kHz. Each spectrum was acquired with 512 points, corresponding to a spectral range of 100 G, then corrected for background and baseline, and normalized following reported procedures.[10]

S1.7.2: Spectral Simulations

To obtain an estimate of the fraction of immobilized population presented in the cw-EPR spectra of dCas9-bound DNAs, the measured spectra were simulated using the "MultiComponent" package provided by the Hubbell group from UCLA (http://www.biochemistry.ucla.edu/biochem/Faculty/Hubbell/). The program allows simulations of cw-EPR spectra with the microscopic-order-macroscopic-disorder model (MOMD).[11] Two issues have been well-documented for EPR simulation, particularly for those at a single frequency,[12, 13] First, the large number of parameters and the interdependency between them may result in a high degree of degeneracy, so that different parameter sets may yield simulated spectra that fit comparably to a particular experimental spectrum. Second, a simple metric based on minimizing the root-mean-square deviation (RMSD) between measured and simulated spectra should not be the sole judging criterion, as uneven contributions to RMSD from different spectral regions (e.g., the central line region largely outweighs the low- and high-field manifolds due to its much larger amplitude) often lead to loss of key motional features in the simulated spectrum. To address these issues, the following procedure was implemented to minimize the variable fitting parameters while reproducing the key motional features reflected in the measured spectra.

Each measured spectrum was simulated as a two-component spectrum, with both components used the following set of invariant parameters: $\boldsymbol{g}$ tensor (g_x = 2.0078, g_y = 2.0058, g_z = 2.0023), $\boldsymbol{A}$ tensor (A_x = 5.70 Gauss, A_y = 6.00 Gauss, A_z = 36.00 Gauss), the Gaussian inhomogeneous broadening parameter (gib0 = 0.00), the Lorentzian inhomogeneous line-broadening tensor (W_x=0.05, W_y=0.05, W_z=0.05), allowed MOMD orientation (N_{nort} = 15), and basis set truncation parameters (L_{emx} = 14, L_{omx} = 11, K_{mx} = 6, M_{mx} = 2, IPN_{mx} = 2). Simulations were executed in three steps. First, the immobilized component (designated as component 1) was simulated as a slow isotropic motion by varying the isotropic rotational diffusion rate (R_1=R_x=R_y=R_z) to achieve the best match in the apparent hyperfine splitting between the measured and the simulated spectra. Second, the simulated component 1 was scaled to optimally match the magnitude of the observed features (bumps) reporting the apparent hyperfine splitting at the outer wings of the low- and high-field regions. Third, the mobile component (component 2) was simulated as motion under an anisotropy-restricting potential by iteratively varying only the following parameters: the orienting potential coefficient (C_{20}), the diffusion tilt angle (β_D), and the axial-symmetric rotational diffusion rates [R_1=(R_x+R_y+R_z)/3, R_2=R_z-(R_x+R_y)/2; R_3=(R_x-R_y)≡0]. The simulated component 2 was judged by two criteria: (1) the appearance of the splitting in the low-field region, which is the most important characteristic

reflecting motions under an anisotropic potential, and (2) best minimizing the discrepancy between the overall measured and simulated spectra (i.e., sum of components 1 and 2).

S1.8: Double Electron-Electron Resonance (DEER) spectroscopy

To prepare a DEER sample, 15 µL of the concentrate from the EPR sample preparation (see S1.6) was combined with an equivalent amount of 80% (v/v) glycerol in buffer R. The mixture was then loaded into a quartz capillary (2.0mm ID x 2.4mm OD, Fiber Optic Center, Inc.) sealed at one end, flash frozen by submersion in liquid nitrogen, and used immediately for data acquisition. The spin-labeled DNA concentration in these samples was approximately 75–100 µM.

DEER data were acquired at 78 K on a Bruker ELEXSYS E580 X-band spectrometer equipped with a MD4 resonator. Previously reported acquisition parameters and procedures[14] were used. Specifically, a dead-time free four-pulse scheme was used,[15] with the pump pulse frequency set at the center of the nitroxide spectrum and the observer frequency approximately 70 MHz lower. The observer π pulse was 32 ns, and the pump π pulse was optimized using a nutation experiment, usually set at 14 ns. The video bandwidth was fixed at 20 MHz. The shot repetition time was set at 1000 µs. Accumulation time in each measurement was approximately 24 hours with 100 shots per point.

Inter-spin distance distributions were computed from the measured dipolar evolution data using the DeerAnalysis2013 program.[16] The reported inter-spin distance distributions were obtained with the Tikhonov regularization approach, and the echo evaluation data were processed with a 1.6-nm long-pass filter. Similar to previous reports,[8] repeat measurements and analyses on variations in the fitting parameters (zero time, background range, and phase) showed that errors in reported most probable distance values were < 10%.

S1.9: Model building and Molecular Dynamics simulations

An initial model of a nucleic acid-bound ternary complex of Cas9 containing a 24-nucleotide non-target DNA strand was built from a co-crystal structure containing Cas9, sgRNA, the target DNA strand, and a non-target DNA strand of only 12 nucleotides (PDB ID 4UN3[17]). The extension of the non-target strand DNA was modeled onto a previously identified positively-charged patch located between the HNH and RuvC nuclease domains of Cas9[18] using PyMol (The PyMOL Molecular Graphics System, Version 1.8 Schrödinger, LLC). The nucleotides were placed at sterically and electrostatically plausible positions, and when possible, hydrogen bonding distances between the DNA backbone and positively charged amino acid residues were maintained. DNA coordinates were generated using 3DNA[19] and sculpted into 4UN3.

The initial model was subjected to all-atom Molecular Dynamics (MD) simulations carried out in explicit solvent with 94 neutralizing Na^+ ions. The water molecules in the unmodified PDB structure 4UN3 were removed, then solvent molecules and ions for simulations were added using the gmx solvent and genion modules of gromacs 5.0.4.[20] The system was solvated in the TIP3P water model and placed in an orthorhombic box with a minimal distance of 10 Å of solute from the box border. The amber99sb force field[21] was used for the rest of the system. Note that while AMBER parmbsc0[22] or later versions[23, 24] are the more stable variant of the AMBER force field, in our study the DNA is embedded in a large ternary complex with the protein and RNA providing structural constraints, and we did not observe any artifacts in the conformational sampling with the amber99sb force field over the extended time span of 1.5 µs (see section S2.7.1).

The MD preparation and production runs were performed using 4 NVIDIA K80 GPUs on a lab-owned server, using gromacs 5.0.4. Periodic boundary conditions were defined by the PME algorithm and the non-bonded cut-off was set to 9 Å, the LINCS fourth-order algorithm was used to constrain hydrogen atoms with a maximum accepted rotation of 60 degrees, and the integration time step was 2fs.[14] The temperature of 300 K was maintained with the velocity rescaling algorithm.[25] The pressure of 1 atm was maintained with the Parrinello-Rahman barostat.[26]

Prior to MD production, a sequence of minimization and equilibration steps were applied. The system was first minimized with 5000 steps of steepest descent. It was then heated at constant volume from 0 to 100 K for 1 ns with randomly generated starting velocities; from 100 K to 200 K for 1 ns and from 200 K to 300 K for 1 ns with starting velocities from the previous equilibration. The system was finally equilibrated for 6.5 ns at constant temperature of 300 K and pressure of 1 atm. The final production run was carried out for continuous 1.5 µs and the frames were written at every 1 ps for the system excluding water and every 20 ps for the entire system. Clustering analysis of the trajectory was carried out with gromacs tools using one frame every 100 ps, with least squares fit and Root-Mean-Square Deviation (RMSD) calculations carried out on the DNA non-target strand. RMSD and atomic distances were evaluated with VMD[27] using one frame every 200 ps.

The NASNOX program[6, 8] was used to compute the expected inter-R5a distances on the MD frames, following procedures and parameters reported previously.[14] Analyses were carried out using one frame per 200 ps, with the labels attached at sites equivalent to c33 and n26, namely at the phosphate between nucleotides 13 and 14 upstream of the PAM on the target strand and at the phosphate between nucleotides 11 and 12 upstream of the PAM on the non-target strand. The R5a labels were not present in the MD simulations because the compatibility of the reported force field for the label[28] has not been thoroughly tested yet for long simulations. The NASNOX algorithm suitably accounts for all sterically allowed orientations of the probes,[6, 8] and has been validated in studies of a protein-DNA complex.[29]

S2. Additional Data

S2.1. Characterization of Cas9 proteins

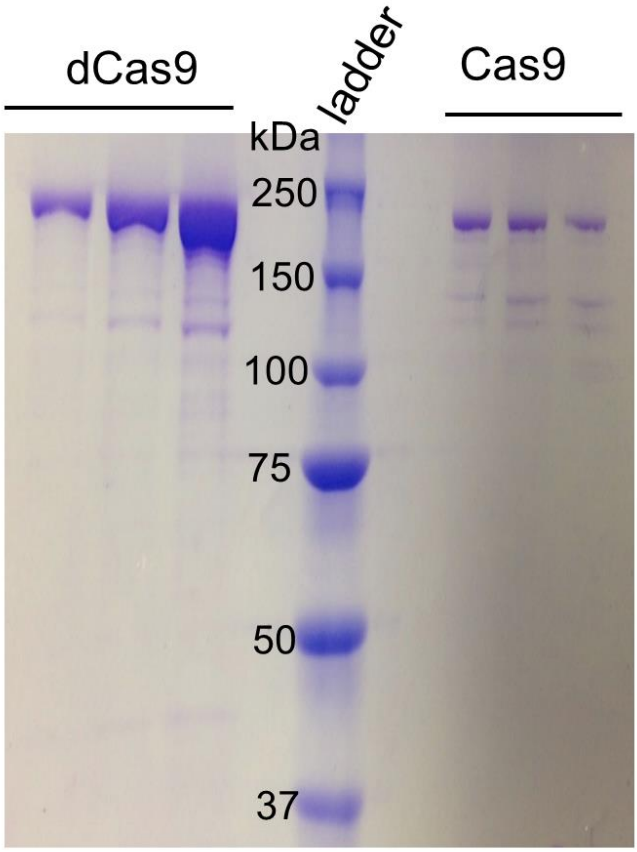

Figure S1: Representative examples of SDS-PAGE of fractions from cation-exchange purification of wild type Cas9 and the catalytically inactive dCas9. The proteins showed the expected size of 198 kDa, which includes the Cas9 protein with the His_6 and MBP tag.

S2.2. Additional biochemical characterization

S2.2.1. Specificity of DNA target recognition

Figure S2B shows results of dCas9/sgRNA binding to two DNA duplexes. As shown, dCas9 super-shifted the sgRNA (Figure S2B lanes 1 and 2), revealing formation of the protein/RNA complex. Upon addition of the p5 duplex, which contains the PAM and the correct protospacer (main text Figure 1), migration of the dCas9/sgRNA complex was accelerated (Figure S2B lane 3), consistent with formation of the ternary dCas9/sgRNA/DNA complex. However, upon addition of the p2 duplex (Figure S2A), which has an appropriate PAM but a protospacer sequence that does not pair with the guide-segment of the sgRNA, little change in the migration of the protein/RNA complex was observed (Figure S2B lane 4), indicating a lack of DNA binding. The data demonstrate the expected requirement of complementarity between the protospacer and the sgRNA for DNA recognition by CRISPR-Cas9.

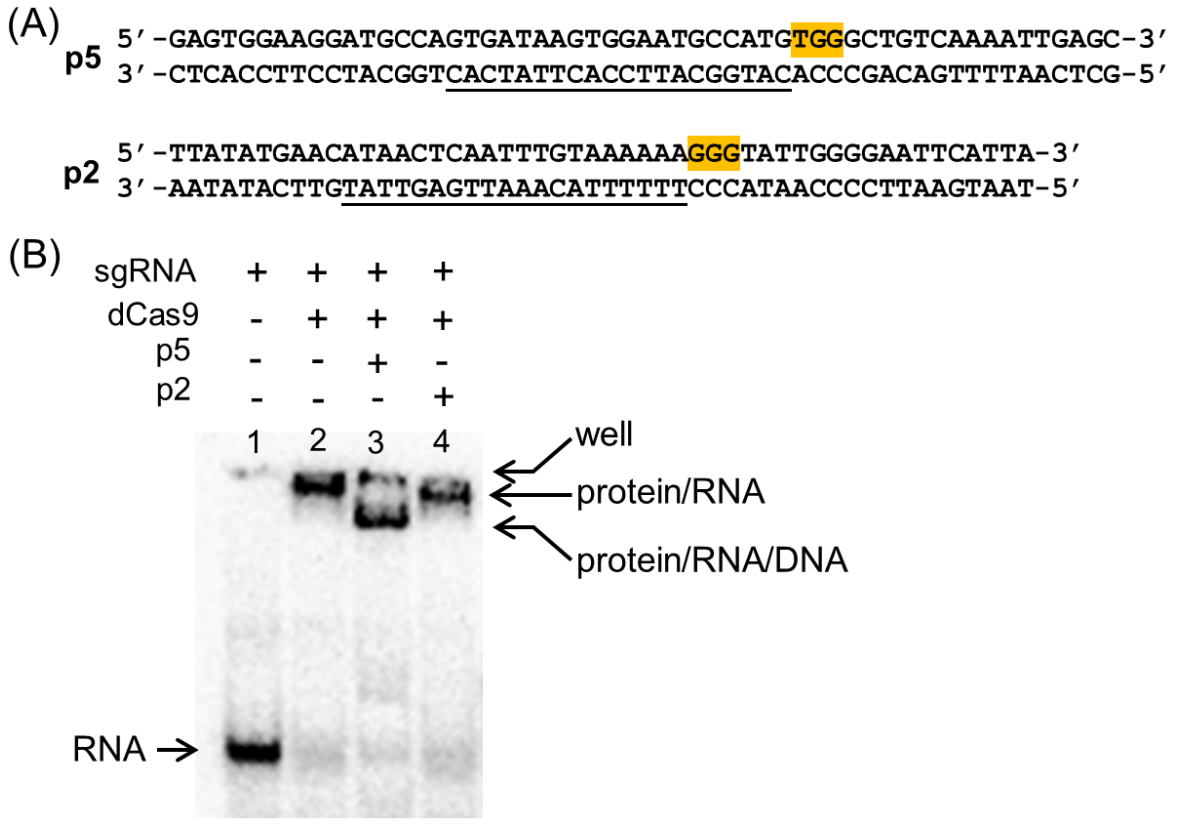

Figure S2: DNA binding by dCas9/sgRNA requires the correct protospacer. (A) Sequences of the p5 (top) and p2 (bottom) DNA duplexes, with PAM highlighted in yellow, and the expected protospacer sequence underlined. (B) Binding of sgRNA and DNA by dCas9 as detected by native gel shift. The samples were assembled with 0.2 μM sgRNA, 0.3 μM DNA, and 0.3 μM dCas9 following procedures described in S1.4. The sgRNA was doped with 5' ^{32}P-labeled sgRNA to allow visualization by auto-radiography.

S2.2.2. Target DNA cleavage requires both sgRNA and an active Cas9

Figure S3 presents control experiments showing that p5 duplex DNA cleavage was absent if: (i) only sgRNA was present (Figure S3, lanes 2 and 8); (ii) only protein was present (Figure S3, lanes 3, 5, 9, and 11); and (iii) the catalytically active Cas9 was substituted with the catalytically inactive dCas9 (Figure S3, lanes 4 and 10). This demonstrates that, as expected, target DNA cleavage required an active Cas9/sgRNA complex.

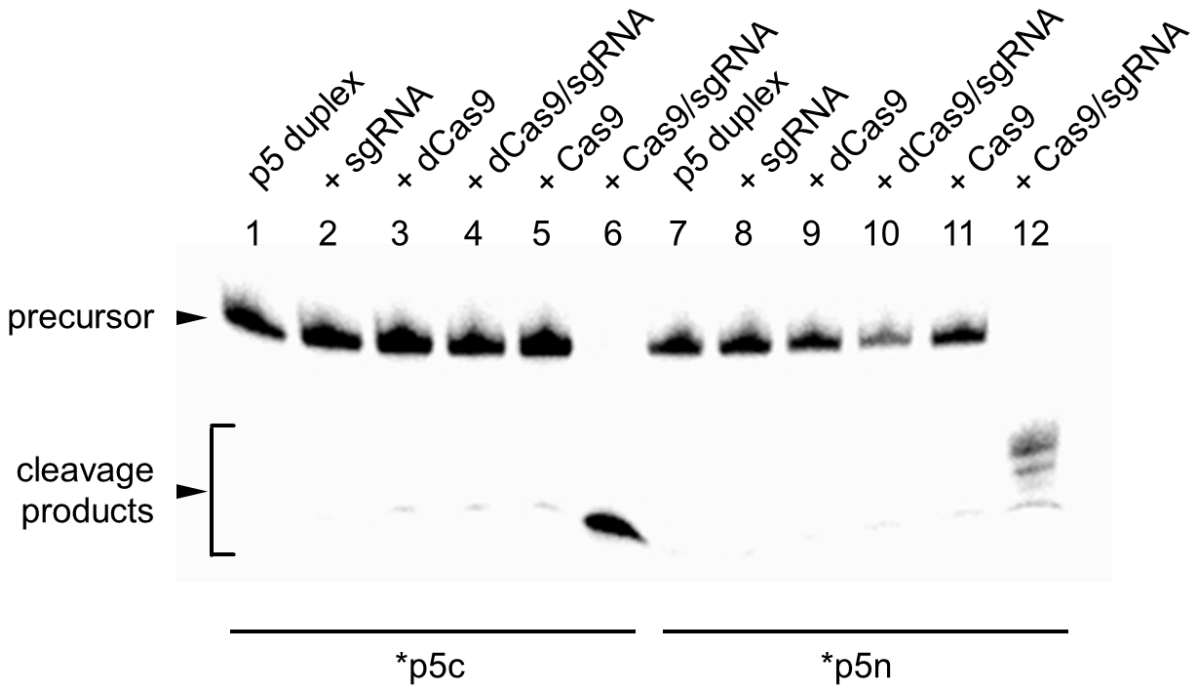

Figure S3: DNA cleavage detected using denaturing PAGE. The experiments were carried out as described in Materials and Methods. Samples were assembled with 100 nM p5 duplex, 300 nM sgRNA, and 500 nM protein. Lanes 1−6 monitored cleavage of the p5c strand that is complementary to the guide-segment of the sgRNA, while lanes 7−12 monitored the p5n strand that is non-complementary to the RNA guide.

S.2.2.3. Cleavage of singly-R5a-labeled DNA duplexes

Figure S4 shows results on Cas9 cleavage of singly-R5a-labeled duplexes. For cleavage of the p5c strand, both R5a-labeled c19 (Figure S4, lane 3) and c33 (Figure S4, lane 4) strands were cleaved to completion, similar to that of the unlabeled DNA (Figure S4, lane 2). Note that with the ^{32}P label at the 5' terminus of the c-strand, the ^{32}P-labeled c19 cleavage product contained an attached R5a, and therefore migrated slightly slower compared to a c-strand without R5a attached (Figure S4, lanes 2 and 3). On the other hand, for the c33 strand, the ^{32}P-labeled product did not have the R5a attached, and migrated with the same rate compared to the unlabeled DNA (Figure S4, lanes 2 and 4). These data indicate R5a labels at c19 and c33 did not interfere with DNA cleavage.

For cleavage of the p5n strand (Figure S4, lanes 5 and 6), R5a-labeled n26 was cleaved to completion, and products migrate with the same rate as that of the unlabeled DNA because the R5a label was not expected to be attached to the ^{32}P-labeled products. The relative distribution of the n26 cleavage products showed a slight difference from that of the unlabeled DNA. This indicates that R5a labeled at n26 did not impact the initial cleavage of the n-strand, but may have an effect as the n-strand is being trimmed towards the n26 labeling site.

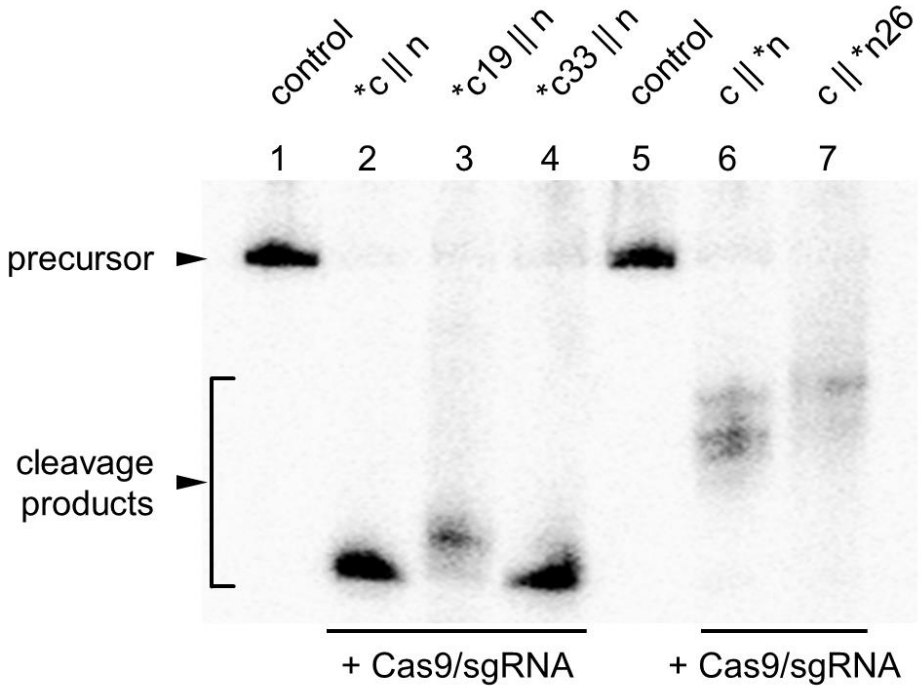

Figure S4: DNA cleavage of singly-spin-labeled duplexes detected using denaturing PAGE. The experiments were carried out as described in Materials and Methods. Samples were assembled with 100 nM p5 duplex, 400 nM sgRNA, and 900 nM Cas9. The ^{32}P-labeled strand is indicated by an asterisk (*). Lanes 1−4 monitored cleavage of the p5c strand (denoted by *c), while lanes 5−7 monitored the p5n strand (denoted by *n). Spin labeling sites are indicated in labels above each lane.

S2.3: Native gel shift analysis of EPR samples

Figure S5 shows results from native gel shift analyses of the actual EPR samples. The results indicate that the spin-labeled DNA was completely bound by the dCas9/sgRNA complex in the EPR measurements.

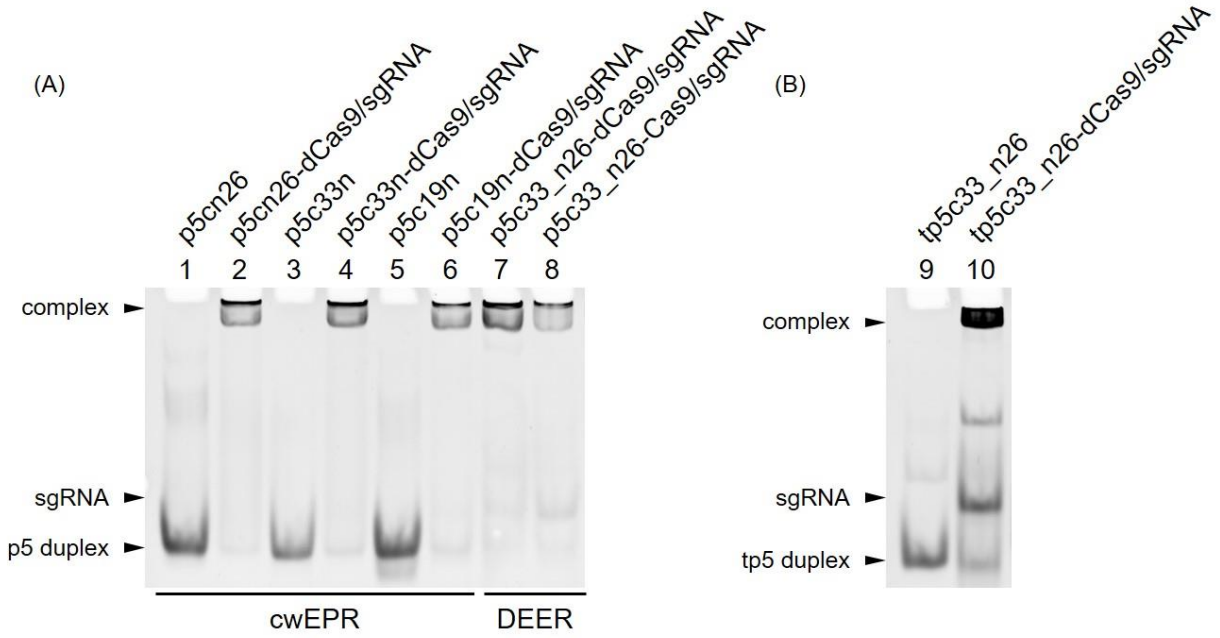

Figure S5: Native gel shift analysis of EPR samples, with nucleic acid species visualized by EtBr staining. (A) Full duplex (p5). Lanes 1−6: singly-R5a labeled p5 duplexes used in cw-EPR measurements; Lanes 7−8: doubly-R5a labeled p5 duplexes used in DEER measurements. (B) Doubly-R5a labeled truncated duplexes (tp5) used in DEER measurements.

S2.4: Binding of singly-spin-labeled DNAs by dCas9 analyzed using cw-EPR spectroscopy

X-band continuous-wave (cw-) EPR spectra of singly-R5a-labeled p5 duplexes were obtained as described above (SI section S1.7). In the unbound state, all three spectra showed closely spaced splitting at the low- and high-field manifolds (Figure S6A). These features have been observed previously, and reveal that the R5a label undergoes anisotropic rotations in the confines of the DNA duplex.[30] Upon binding by dCas9/sgRNA (SI section S2.3), spectral broadening was observed (Figure S6B), indicating binding of DNA by the dCas9/sgRNA complex.

For the c19 label located opposite the PAM sequence, the bound spectrum showed broad, multiple component features (Figure S6B), indicating extensive contacts with the protein and/or RNA. This is unexpected given current reported structures,[17] although here the constructs differ from the reported structures in that the entire non-target strand is present, and the protein includes the purification tags. Thus, c19 was not included for distance analyses, as these extensive contacts render it difficult to assess whether distance changes would have arisen from DNA conformation or R5a rotamer alterations.

Figure S6: Normalized cw-EPR spectra of R5a-labeled p5 in the (A) unbound and (B) dCas9/sgRNA bound states.

For n26 and c33, spectral simulations were able to generate satisfactory fits to the spectra obtained for dCas9-bound complex (Figure S7). The simulations showed that each of the measured spectra could be accounted for by a mobile and an immobile component. The mobile component, which accounted for 75% and 82% of the total population for n26 and c33, respectively (Figure S7), maintained closely-spaced splittings at the low- and high-field

manifolds, indicating that the nitroxides maintained the anisotropic rotational motion as observed in the free duplex. This suggests that at n26 and c33, upon dCas9 binding, the majority of nitroxides remains free of contacts to the protein/RNA complex.

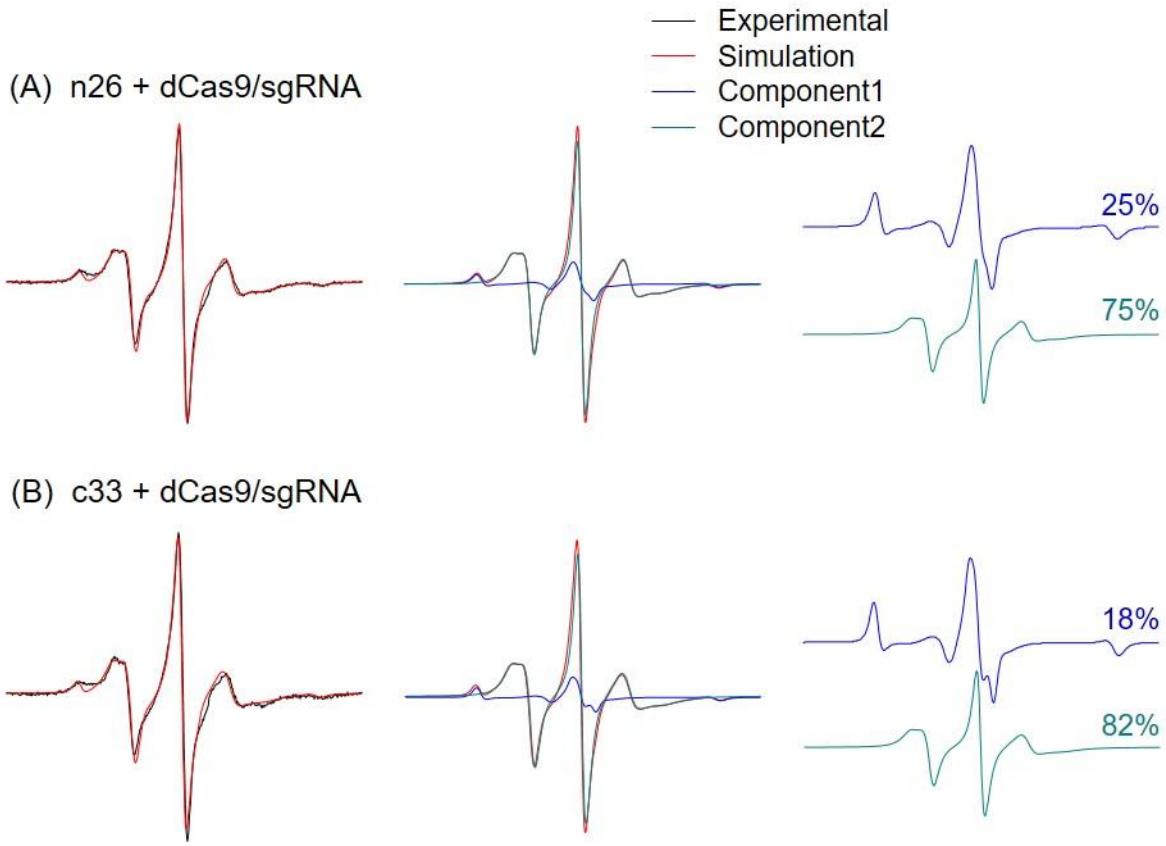

Figure S7: Simulations of cw-EPR spectra for Cas9-bound DNA duplexes with a single R5a attached at n26 (panel A) or c33 (panel B). In each panel, shown on the left are the overlaid of measured spectrum (black) and the overall simulated spectrum (red); in the center is the overall simulated spectrum (red), overlaid with simulated component 1 (blue), and simulated component 2 (green); and on the right are the individual component 1 and 2 spectra, normalized to the same center-line height for comparison, with the respective percent contribution listed. In addition to the invariant parameters described in Materials and Methods (S1.7.2), values of the fitted parameters for the simulated spectra shown are: n26-labeled duplex, $\log_{10}(R)=6.60$ for component 1 and $C_{20}=2.69$, $ß_D=42.29$, $\log_{10}(R_1)=7.84$, and $\log_{10}(R_2)=1.30$ for component 2; c33-labeled duplex, $\log_{10}(R)=6.45$ for component 1 and $C_{20}=2.10$, $ß_D=40.00$, $\log_{10}(R_1)=8.11$, and $\log_{10}(R_2)=1.11$ for component 2.

S2.5: Additional DEER data

S2.5.1: Raw DEER traces

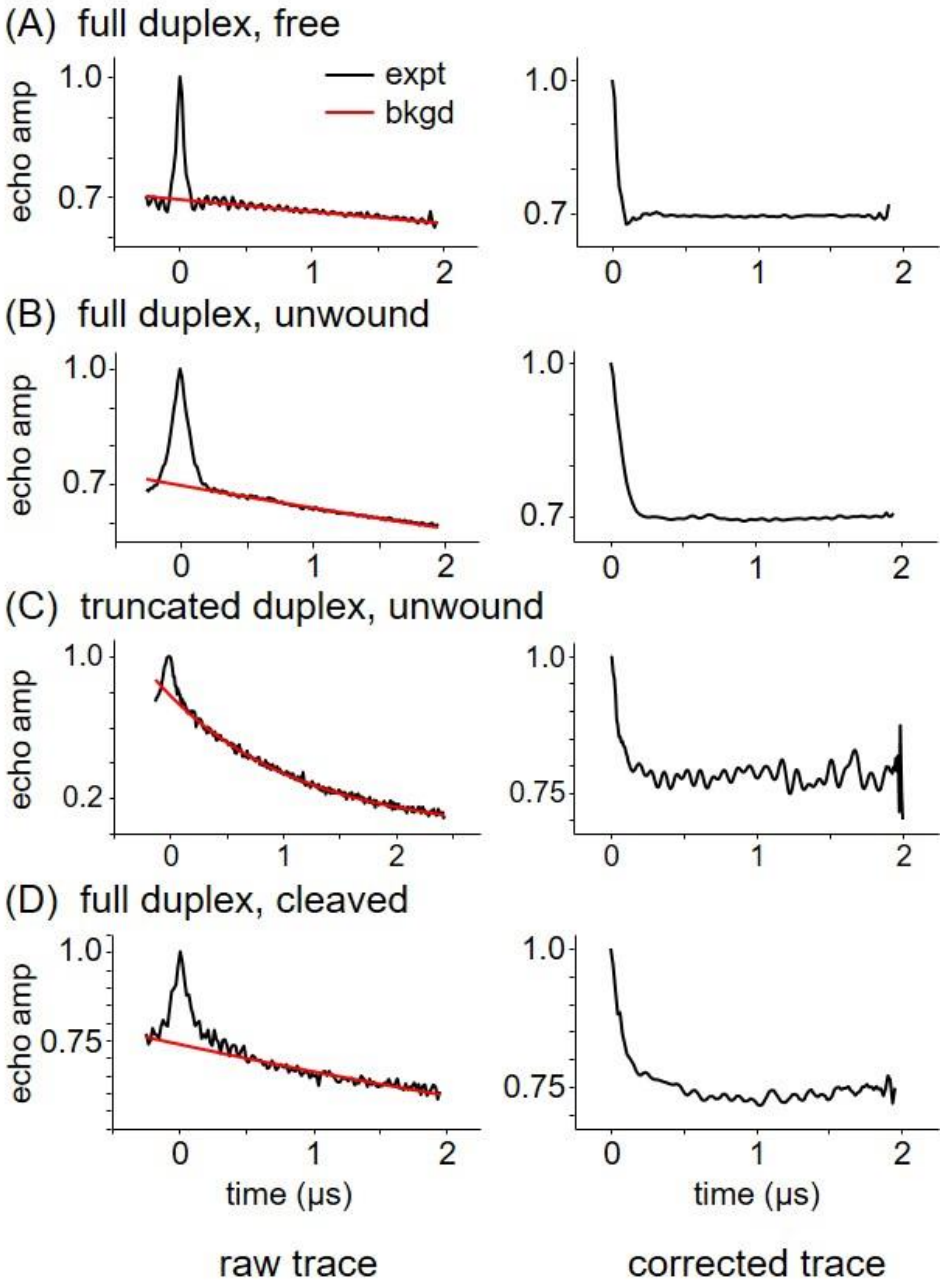

Figure S8: Original DEER traces for the c33_n26 duplex measured in various states. In each panel, raw traces are shown on the left in black, with the selected background in red, and background-corrected traces are shown on the right. (A) Unbound full duplex formed with p5n26 and p5c33 DNA strands (Table 2). (B) Full duplex bound and unwound by dCas9. (C) Truncated duplex (formed with tp5n26 and p5c33 DNA strands, Table 2) bound and unwound by dCas9. (D) Full duplex bound and cleaved by Cas9.

S2.5.2: DEER measurement of free truncated target DNA duplex

Figure S9 shows the c33_n26 inter-spin distance measured in the absence of Cas9/sgRNA in the truncated p5 duplex formed between the R5a-labeled p5c33 and tp5n26 strands (Table S2). The resulting distance of 21 Å for the truncated duplex (Figure S9B) is consistent with that of the unbound full-length duplex (main text, Figure 3A), indicating the expected formation of the truncated duplex.

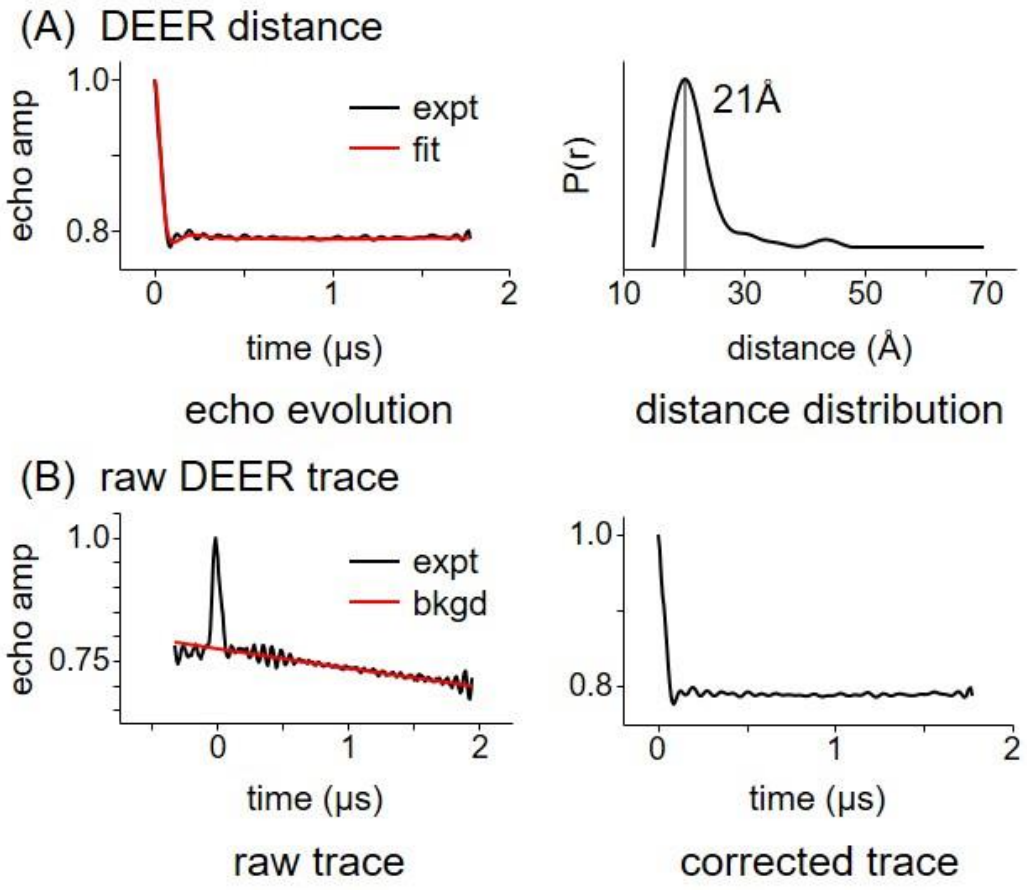

Figure S9: DEER data for the unbound c33_n26 truncated DNA duplex. (A) The echo evolution is shown on the left in black, with the Tikhonov-calculated fit overlaid in red, and the resulting distance distribution is shown on the right, with the most probable DEER distance of 21 Å marked. (B) The raw trace is shown on the left in black, with the selected background in red, and the background-corrected trace is shown on the right.

S2.6: Assessment of multiple DEER distance populations

For the full duplex (i.e., duplex formed with p5n26 and p5c33, Table S2) in its dCas9 bound and unwound state, the n26_c33 inter-spin distance distribution computed using the Tikhonov regularization approach (see Materials and Methods) showed the most probable distance of 27 Å and a minor component at 44 Å (main text, Figure 3B). The validity of these populations was further evaluated using the DEERconstruct program developed by the Fanucci group.[31] In brief, the Tikhonov-generated distance distribution profile was reconstituted with multiple Gaussians. Dipolar evolution traces were then produced by suppression of one or more of the previously defined Gaussians, and the newly constructed traces were compared to the original trace using a statistical test. As shown in Figure S10A, the analyses reported that the 44-Å component accounts for only 5.7% of the total population, and tests based on standard deviation and variance both indicate that this component is insignificant. Therefore, this component was considered an artifact.

In the case of the truncated duplex (i.e., duplex formed with tp5n26 and p6c33, Table S2) in its dCas9 bound and unwound state, the computed distance distribution profile showed two major populations, centered at 22 Å and 35 Å, and another very minor at 44 Å (main text, Figure 3C). The 35-Å component was determined to account for 17.7% of the total population, and analyses of standard deviation and variance reveal that this population is significant (Figure S10B). The same analysis of the very small population at 44 Å resulted in its characterization as an artifact (data not shown).

The full duplex in its Cas9 bound and cleaved state yielded an inter-spin distance distribution showing two major populations, with most probable distances at 26 Å and 44 Å (main text, Figure 3D). Statistical analyses, as described above, showed that the 44-Å component accounts for 21.6% of the total population, and both standard deviation and variance identify this component as significant (Figure S10C).

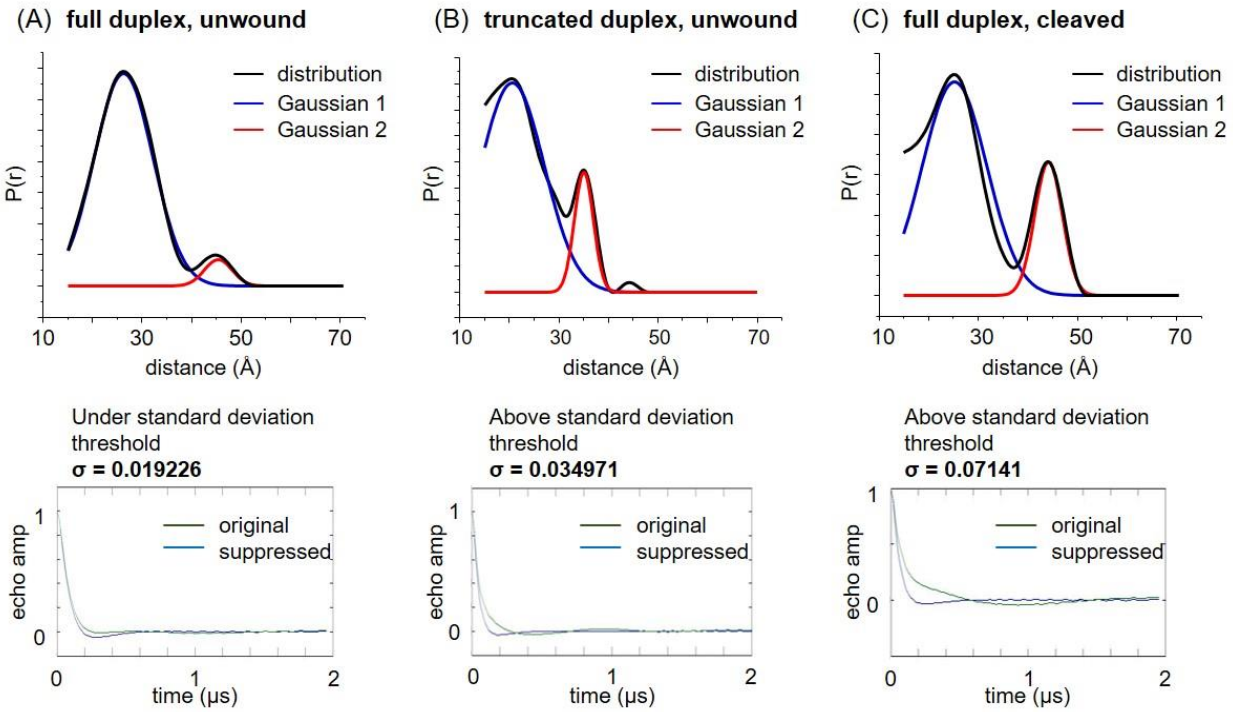

Figure S10: Analysis of the multiple populations in the distance distributions shown in Figure 3 in the main text. In each panel, shown on top is the overlay of the distance distribution and its Gaussian components, and shown at the bottom is the comparison between the original dipolar evolution trace (green) and its counterpart (blue) calculated based on the suppression of a Gaussian component. (A) Full duplex in its daCa9 bound and unwound state. (B) Truncated duplex in its dCas9 bound and unwound state. (C) Full duplex in its Cas9 bound and cleaved state.

S2.7: Additional analysis of MD simulations

S2.7.1. System stability during the MD simulation

Figure S11 shows the RMSD over the heavy atoms of the entire ternary system (DNA+Cas9/RNA) over the 1.5 µs (or 1,500 ns) MD trajectory. Although the plot reveals residual fluctuations, over the course of entire trajectory no steady drift is detected, indicating a fair stability of the system during simulation.

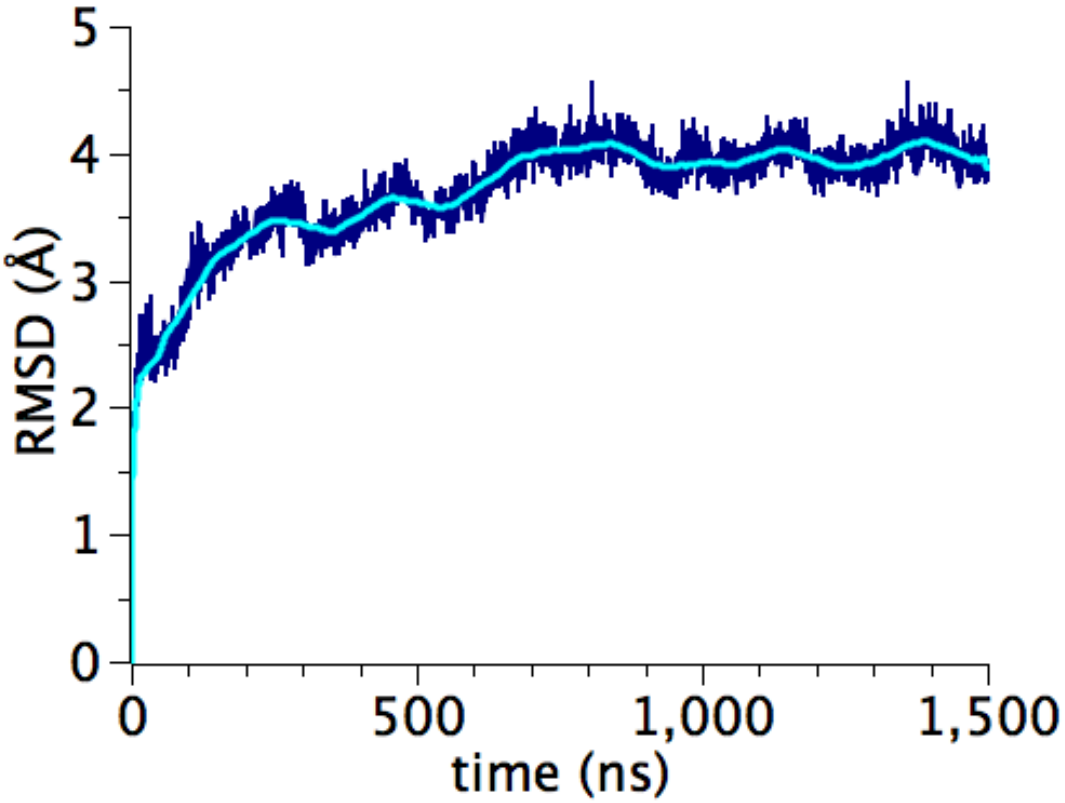

Figure S11: RMSD over the heavy atoms of the entire ternary system (DNA+Cas9/RNA). The raw trace is shown in blue, and the RMSD smoothed over a time window of 100 ns in cyan. RMSD calculations were based on alignment of the Cas9 protein backbone.

S2.7.2: Time-dependence of the inter-R5a distance

Figure S12 shows the trace of inter-R5a distances over the entire time span of the MD simulation. The R5a-R5a distances were obtained by applying NASNOX to the MD snapshots, with the R5a labels modeled at the nucleotide positions equivalent to c33 and n26 shown in Figure 1 in the main text (see also S1.9). The initial segment of the trace (0 to ~462 ns) fluctuated around an average of 28.7 Å, corresponding to the shorter distance peak of Figure 4B in the main text. This stable initial segment covered the entire span (138 to 462 ns) during which the conformation of the non-target strand fell into the second most populated cluster (Table S3, section S2.7.3). A transition (~500 to 650 ns) then followed, roughly corresponding to the time span of the third most populated cluster (Table S3). For the remaining portion of the trace, during which the conformation of the complex was classified as the most populated cluster (Table S3), the inter-R5a distance first fluctuated around a plateau corresponding to the longer distance peak at 32.6 Å in main text Figure 4C, then gradually decreased towards the 28.7-Å value observed initially.

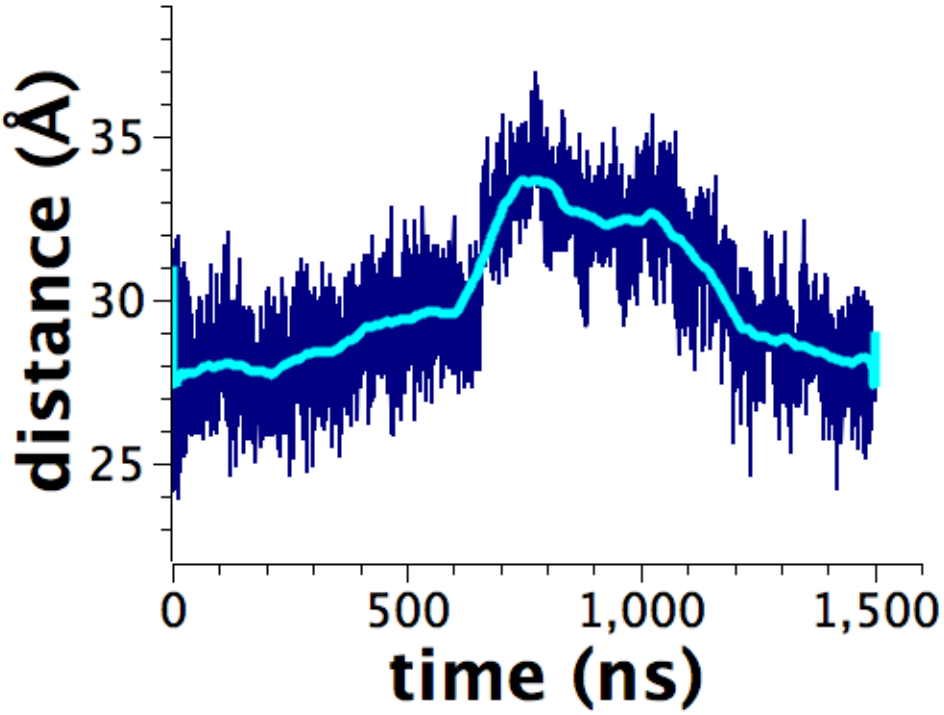

Figure S12: R5a-R5a distance as a function of time during the entire simulation length (blue, 1 frame every 200 ps) and smoothed signal (cyan) over a 100 ns window.

S2.7.3: Analyses of flexibility in the non-target DNA strand

To examine variations of the non-target DNA conformation in the MD trajectory, clustering analysis was carried out, and the top three most populated clusters identified are listed in Table S3. Comparisons between the most representative structures from the top two most populated clusters (Figure 4A in the main text) showed that the non-target strand of the DNA displays the highest RMSD among the various elements of the ternary complex (Figure S13), indicating that the non-target strand of the DNA has the highest flexibility. In addition, different segments of the non-target strand showed large variations in their RMSD values (Figure S13B), suggesting that dynamic characteristics differ among the different segments. This is consistent with the partial RMSD traces for different segments of the non-target strand plotted throughout the entire MD trajectory (Figure 4C in the main text).

Table S3: Population and time extension of three most populated structural clusters

Cluster	No. of structures (population)	Centroid frame (ns)	Time range (ns)
1	8086 (54%)	1017.9	651 – 1495
2	2745 (18%)	310.9	138 – 462
3	1458 (10%)	600.4	504 – 651

To further assess dynamics in the non-target strand in a reference-independent manner, distances were calculated between P of each nucleotide in the non-target strand and Cα of the 22 residues that compose the positively charged patch (at the interface between RuvC and HNH) and a few others in the PAM-Interacting domain (PI) of Cas9, as identified by Slaymaker, Zhang and coworkers.[18] These distances were analyzed in order to identify differences in flexibility along the non-target strand, as well as to clarify structural distinction between the clusters. Figure S14 shows a representative plot of one of these DNA-protein distances. There was clearly a transition in the time span of the third most populated cluster, which accounts for the separation between the first and second clusters. The inspection of individual time traces of distances between DNA nucleotide and protein residue showed similar behavior for different atom pairs.

To obtain a more global description, contact distance maps were generated by averaging the distances for each P-Cα pair over the time spans of the two most populated clusters (Figure S15). The absolute value of the difference between the maps for the top two most populated clusters (Figure S16) showed overall small changes for nucleotides down-stream of the PAM that are duplexed (i.e., Figure S13A, −1 to −8), although exceptions could be seen between the DNA and K862 in HNH and R976 in RuvC (Figure S16). Larger variations were observed for nucleotides in the unwound protospacer (i.e., +1 to +16, Figure S16), with particularly large differences near the 5' terminus (i.e., the PAM-distal segment, Figure S16). Further inspection showed that the positively charged patch is located closer to the PAM-proximal fragment (Figure S15). The electrostatic interactions between the negatively charged backbone of PAM-proximal segment and the positively charged RuvC/HNH interface stabilize the DNA conformation.

Overall, analyses of clusters, partial RMSD, and contact maps support the conclusions that dynamics of the unwound non-target strand varies between different segments, with the highest flexibility at the distal segment with respect to the PAM.

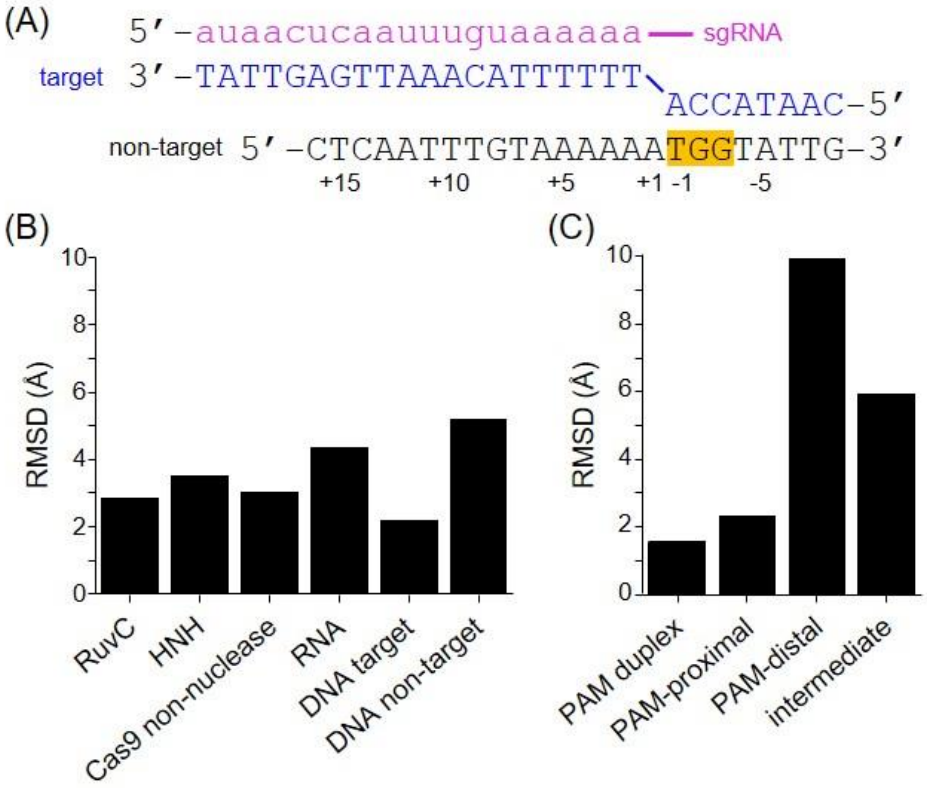

Figure S13: Comparisons between the two most representative structures shown in Figure 4A in the main text. (A) Nucleotide sequences in the model used in the MD simulation. The PAM is highlighted in yellow, and numbering of the non-target strand with respect to the PAM is shown, with nucleotides +1 to +16 upstream of PAM being the unwound protospacer. (B) Partial RMSD on different portions of the ternary complex. RMSD was computed based on alignment of the Cas9 protein in the ternary complex. (C) Partial RMSD on different portions of the non-target DNA strand. Different segments are designated with reference to numbering shown in panel (A): PAM duplex, nucleotides -1 to -8; PAM-proximal, nucleotides +1 to +8; intermediate, nucleotides +9 to +11; PAM-distal, nucleotides +12 to +16.

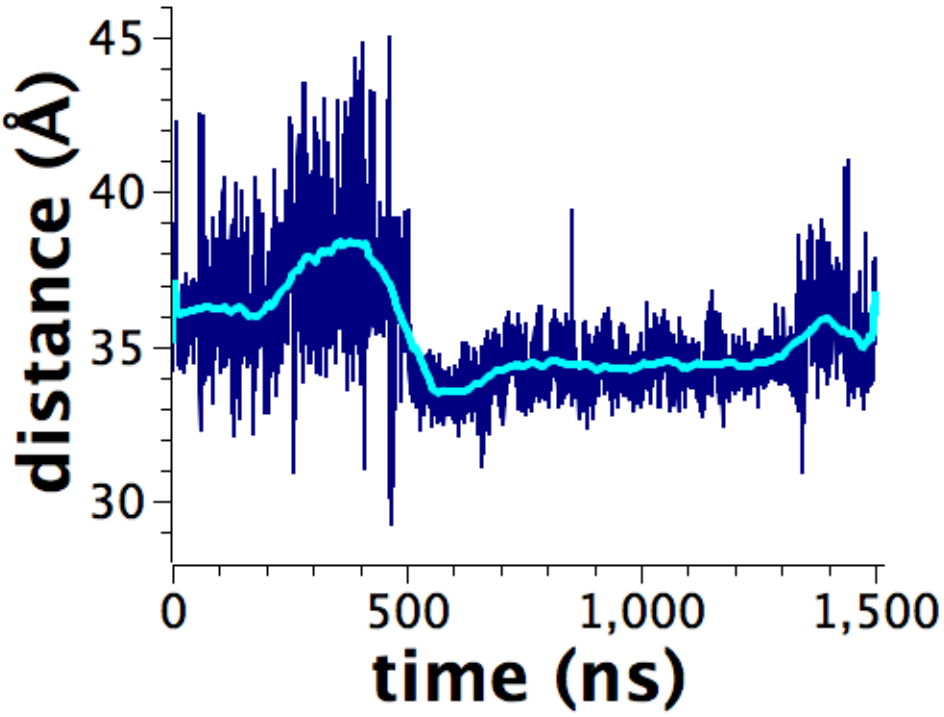

Figure S14: Distances between the P atom of the 15th nucleotide upstream of the PAM (i.e., the P atom of the phosphate between T15 and C16, Figure S13A) and the Cα atom of residue K855 in the HNH protein domain, plotted as a function of time during the entire simulation length. The raw trace is shown in blue, and the RMSD smoothed over a time window of 100 ns in cyan. The initial portion, covering the second most populated cluster (138–462 ns), is characterized by quite large fluctuations. The final portion, covering the most populated cluster, is characterized by sensibly smaller fluctuations and a smaller average distance.

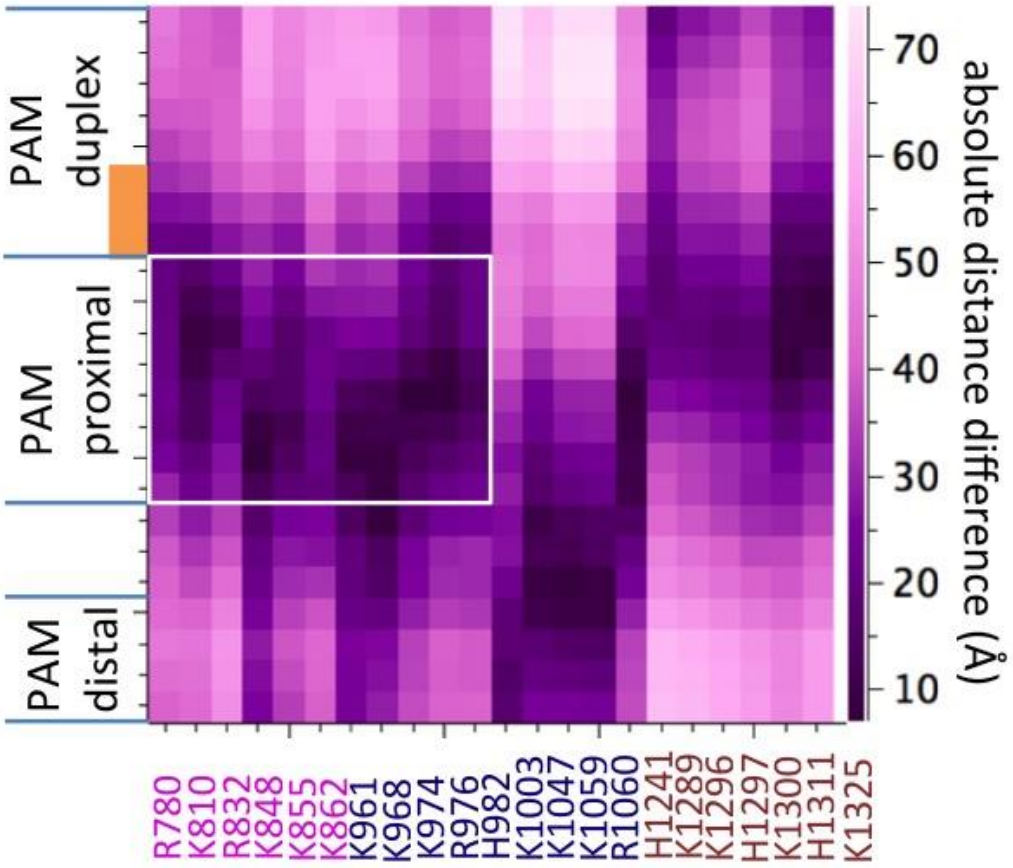

Figure S15: Contact distance map between the non-target strand of DNA and Cas9 protein obtained for the most populated cluster. The vertical axis shows nucleotides of the non-target DNA strand, with the PAM marked in orange. Different segments are marked with reference to numbering in Figure S13A as: PAM-duplex, nucleotides -1 to -8; PAM-proximal, nucleotides +1 to +8; PAM-distal, nucleotides +12 to +16. The horizontal axis lists Cas9 residues located at the HNH (magenta), RuvC (blue) and PI (pink) domains, which mark the positively-charged patch.[18] The white rectangle identifies the region of closest contact between the non-target strand and the positively charged patch, which spans the RuvC-HNH interface and the PAM-proximal portion of the non-target DNA strand.

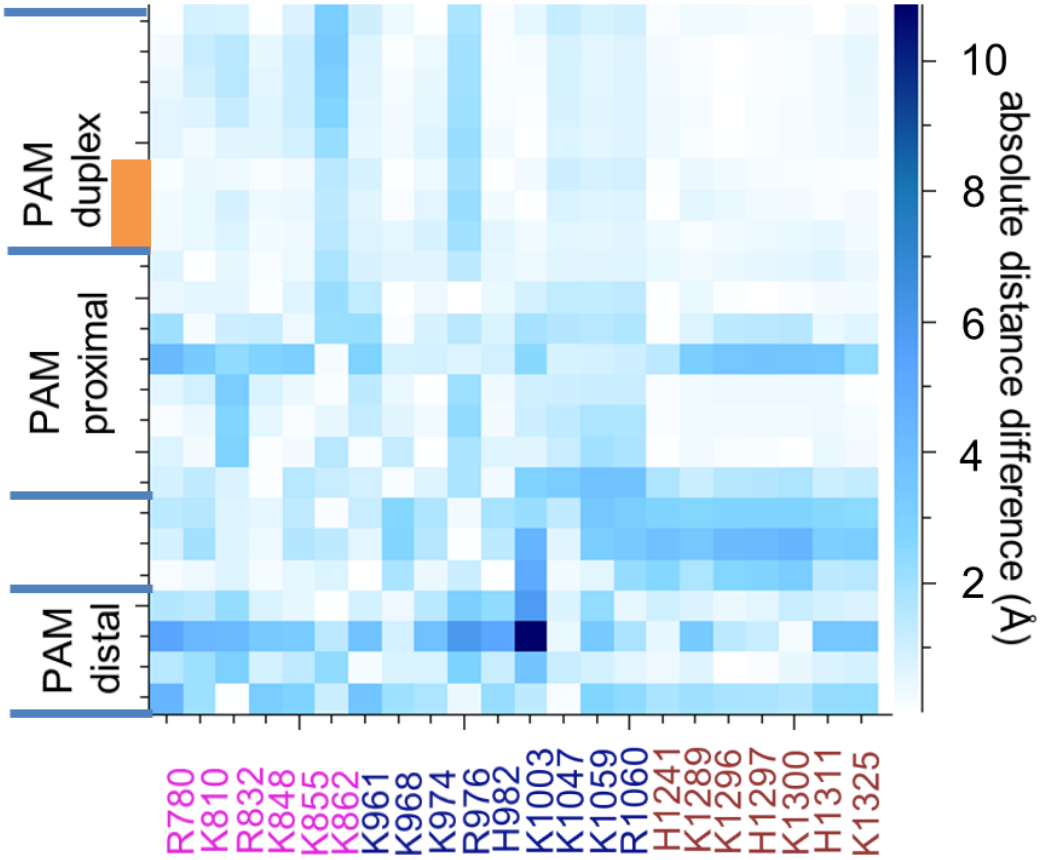

Figure S16: Contact distance difference (absolute value) map between the first and second most populated clusters showing variations in non-target DNA strand conformation. The vertical axis shows nucleotides of the non-target DNA strand, with the PAM identified by the orange rectangle. Different segments are marked with reference to numbering in Figure S13A as: PAM duplex, nucleotides -1 to -8; PAM-proximal, nucleotides +1 to +8; PAM-distal, nucleotides +12 to +16. The horizontal axis lists Cas9 residues located at the HNH (magenta), RuvC (blue) and PI (pink) domains, which mark the positively-charged patch.[18]

S2.8: DNA cleavage in the DEER-measured samples

DEER samples were recovered and electrophoresed on a denaturing gel to assess the degree of cleavage under the DEER measurement conditions. As shown in Figure S17, with the catalytically active Cas9/sgRNA complex, a majority of the p5 DNA was cleaved (70% for c33_n26, Figure S17, lane 2). No cleavage was observed with the catalytically inactive dCas9/sgRNA complex (Figure S17, lane 3).

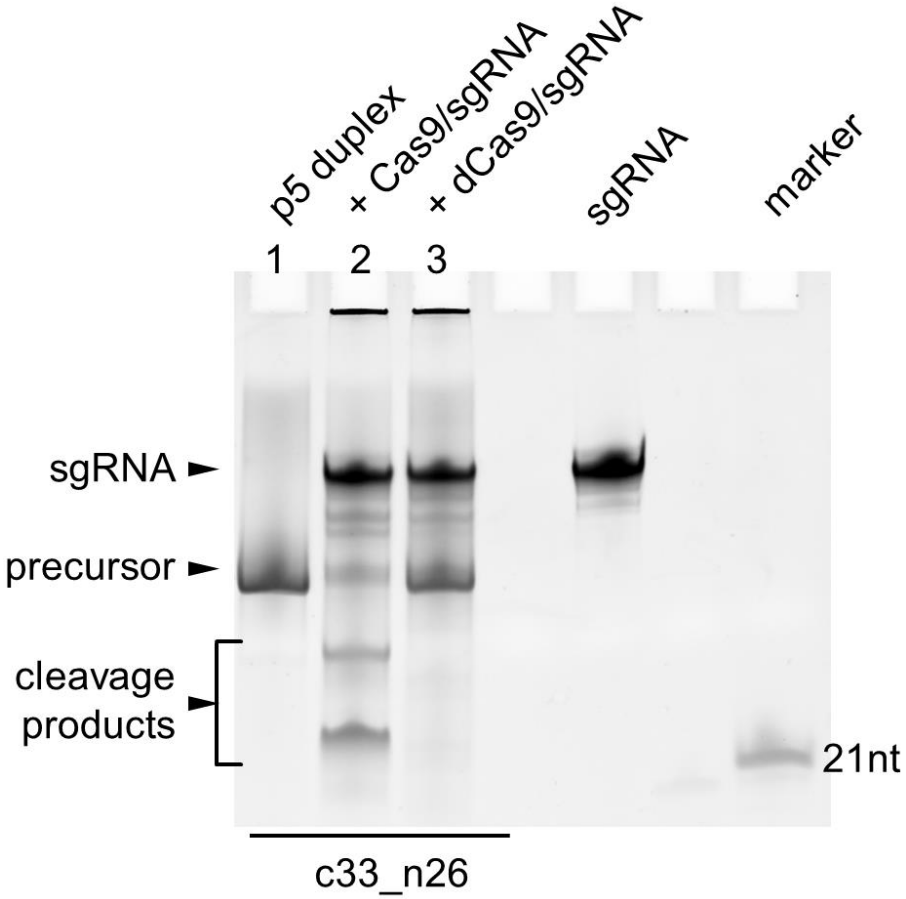

Figure S17: Denaturing PAGE of the DEER-measured samples. Nucleic acid species were visualized with EtBr staining.

References:

1. Jinek, M., Chylinski, K., Fonfara, I., Hauer, M., Doudna, J. A., and Charpentier, E. (2012) A Programmable Dual-RNA–Guided DNA Endonuclease in Adaptive Bacterial Immunity, *Science 337*, 816-821.
2. Anders, C., and Jinek, M. (2014) In Vitro Enzymology of Cas9, In *Method Enzymol.* (Jennifer, A. D., and Erik, J. S., Eds.), pp 1-20, Academic Press.
3. Jinek, M., Jiang, F., Taylor, D. W., Sternberg, S. H., Kaya, E., Ma, E., Anders, C., Hauer, M., Zhou, K., Lin, S., Kaplan, M., Iavarone, A. T., Charpentier, E., Nogales, E., and Doudna, J. A. (2014) Structures of Cas9 Endonucleases Reveal RNA-Mediated Conformational Activation, *Science 343*, 1247997.
4. Nishimasu, H., Ran, F. A., Hsu, Patrick D., Konermann, S., Shehata, Soraya I., Dohmae, N., Ishitani, R., Zhang, F., and Nureki, O. (2014) Crystal Structure of Cas9 in Complex with Guide RNA and Target DNA, *Cell 156*, 935-949.
5. Tangprasertchai, N. S., Zhang, X., Ding, Y., Tham, K., Rohs, R., Haworth, I. S., and Qin, P. Z. (2015) An Integrated Spin-Labeling/Computational-Modeling Approach for Mapping Global Structures of Nucleic Acids, In *Method Enzymol.* (Peter, Z. Q., and Kurt, W., Eds.), pp 427-453, Academic Press.
6. Qin, P. Z., Haworth, I. S., Cai, Q., Kusnetzow, A. K., Grant, G. P. G., Price, E. A., Sowa, G. Z., Popova, A., Herreros, B., and He, H. (2007) Measuring nanometer distances in nucleic acids using a sequence-independent nitroxide probe, *Nat. Protocols 2*, 2354-2365.
7. Qin, P. Z., Butcher, S. E., Feigon, J., and Hubbell, W. L. (2001) Quantitative analysis of the GAAA tetraloop/receptor interaction in solution: A site-directed spin labeling study., *Biochemistry 40*, 6929-6936.
8. Cai, Q., Kusnetzow, A. K., Hubbell, W. L., Haworth, I. S., Gacho, G. P. C., Van Eps, N., Hideg, K., Chambers, E. J., and Qin, P. Z. (2006) Site-directed spin labeling measurements of nanometer distances in nucleic acids using a sequence-independent nitroxide probe., *Nucl. Acids Res. 34*, 4722-4734.
9. Fang, Y., Cai, Q., and Qin, P. Z. (2005) The procapsid binding domain of phi29 packaging RNA has a modular architecture and requires 2'-hydroxyl groups in packaging RNA interaction., *Biochemistry 44*, 9348-9358.
10. Zhang, X., Cekan, P., Sigurdsson, S. T., and Qin, P. Z. (2009) Studying RNA using site-directed spin-labeling and continuous-wave electron paramagnetic resonance spectroscopy., *Method Enzymol. 469*, 303-328.
11. Earle, K. A., and Budil, D. E. (2006) Calculating Slow-motion ESR Spectra of Spin-Labeled Polymers, In *Advanced ESR Methods in Polymer Reaserch* (Schlick, S., Ed.), pp 53-83, John Wiley and Sons, New York.
12. Zhang, Z., Fleissner, M. R., Tipikin, D. S., Liang, Z., Moscicki, J. K., Earle, K. A., Hubbell, W. L., and Freed, J. H. (2010) Multifrequency Electron Spin Resonance Study of the Dynamics of Spin Labeled T4 Lysozyme, *J. Phys. Chem. B 114*, 5503-5521.
13. Columbus, L., Kalai, T., Jeko, J., Hideg, K., and Hubbell, W. L. (2001) Molecular motion of spin-labeled side chains in a-helices: analysis by variation of side chain structure, *Biochemistry 40*, 3828-3846.
14. Zhang, X., Xu, C.-X., Di Felice, R., Sponer, J., Islam, B., Stadlbauer, P., Ding, Y., Mao, L., Mao, Z.-W., and Qin, P. Z. (2016) Conformations of Human Telomeric G-Quadruplex Studied Using a Nucleotide-Independent Nitroxide Label, *Biochemistry 55*, 360-372.
15. Pannier, M., Veit, S., Godt, A., Jeschke, G., and Spiess, H. W. (2000) Dead-Time Free Measurement of Dipole-Dipole Interactions between Electron Spins., *J. Magn. Res. 142*, 331-340.

16. Jeschke, G., Chechik, V., Ionita, P., Godt, A., Zimmermann, H., Banham, J., Timmel, C., Hilger, D., and Jung, H. (2006) DeerAnalysis2006—a comprehensive software package for analyzing pulsed ELDOR data, *Appl. Magn. Reson. 30*, 473-498.
17. Anders, C., Niewoehner, O., Duerst, A., and Jinek, M. (2014) Structural basis of PAM-dependent target DNA recognition by the Cas9 endonuclease, *Nature 513*, 569-573.
18. Slaymaker, I. M., Gao, L., Zetsche, B., Scott, D. A., Yan, W. X., and Zhang, F. (2016) Rationally engineered Cas9 nucleases with improved specificity, *Science 351*, 84-88.
19. Lu, X. J., and Olson, W. K. (2003) 3DNA: a software package for the analysis, rebuilding and visualization of three-dimensional nucleic acid structures, *Nucleic Acids Research 31*, 5108-5121.
20. Hess, B., Kutzner, C., van der Spoel, D., and Lindahl, E. (2008) GROMACS 4: Algorithms for Highly Efficient, Load-Balanced, and Scalable Molecular Simulation, *Journal of Chemical Theory and Computation 4*, 435-447.
21. Hornak, V., Abel, R., Okur, A., Strockbine, B., Roitberg, A., and Simmerling, C. (2006) Comparison of multiple Amber force fields and development of improved protein backbone parameters, *Proteins: Structure, Function, and Bioinformatics 65*, 712-725.
22. Pérez, A., Marchán, I., Svozil, D., Sponer, J., Cheatham Iii, T. E., Laughton, C. A., and Orozco, M. (2007) Refinement of the AMBER Force Field for Nucleic Acids: Improving the Description of α/γ Conformers, *Biophys. J. 92*, 3817-3829.
23. Galindo-Murillo, R., Robertson, J. C., Zgarbová, M., Šponer, J., Otyepka, M., Jurečka, P., and Cheatham, T. E. (2016) Assessing the Current State of Amber Force Field Modifications for DNA, *J. Chem. Theory Comput. 12*, 4114-4127.
24. Ivani, I., Dans, P. D., Noy, A., Perez, A., Faustino, I., Hospital, A., Walther, J., Andrio, P., Goni, R., Balaceanu, A., Portella, G., Battistini, F., Gelpi, J. L., Gonzalez, C., Vendruscolo, M., Laughton, C. A., Harris, S. A., Case, D. A., and Orozco, M. (2016) Parmbsc1: a refined force field for DNA simulations, *Nat Meth 13*, 55-58.
25. Bussi, G., Donadio, D., and Parrinello, M. (2007) Canonical sampling through velocity rescaling, *The Journal of Chemical Physics 126*, 014101.
26. Parrinello, M., and Rahman, A. (1981) Polymorphic transitions in single crystals: A new molecular dynamics method, *Journal of Applied Physics 52*, 7182-7190.
27. Humphrey, W., Dalke, A., and Schulten, K. (1996) VMD: Visual molecular dynamics, *Journal of Molecular Graphics 14*, 33-38.
28. Popova, A. M., Hatmal, M. m. M., Frushicheva, M. P., Price, E. A., Qin, P. Z., and Haworth, I. S. (2012) Nitroxide Sensing of a DNA Microenvironment: Mechanistic Insights from EPR Spectroscopy and Molecular Dynamics Simulations, *J. Phys. Chem. B 116*, 6387-6396.
29. Chen, Y., Zhang, X., Dantas Machado, A. C., Ding, Y., Chen, Z., Qin, P. Z., Rohs, R., and Chen, L. (2013) Structure of p53 binding to the BAX response element reveals DNA unwinding and compression to accommodate base-pair insertion, *Nucl. Acids Res. 41*, 8368-8376.
30. Popova, A. M., Kálai, T., Hideg, K., and Qin, P. Z. (2009) Site-Specific DNA Structural and Dynamic Features Revealed by Nucleotide-Independent Nitroxide Probes, *Biochemistry 48*, 8540-8550.
31. Casey, T. M., and Fanucci, G. E. (2015) Spin labeling and Double Electron-Electron Resonance (DEER) to Deconstruct Conformational Ensembles of HIV Protease, *Methods in Enzymology 564*, 153-187.